ELSEVIER

Polymer 42 (2001) 5307–5319

polymer

www.elsevier.nl/locate/polymer

Free volume and transport properties of heterogeneous poly(ethylene-*co*-octene)s

B. Neway[a], M.S. Hedenqvist[a], V.B.F. Mathot[b], U.W. Gedde[a,*]

[a]*Department of Polymer Technology, Royal Institute of Technology, UWG, SE-100 44 Stockholm, Sweden*
[b]*DSM Research, P.O. Box 18, 6160 MD Geleen, The Netherlands*

Received 6 November 2000; accepted 7 December 2000

Abstract

n-Hexane desorption measurements were performed on heterogeneous poly(ethylene-*co*-octene)s with hexyl branch contents between 0.8 and 3.9 mol% and crystallinities between 30 and 60%. Crystal core contents obtained by Raman spectroscopy were lower than the density-based crystallinity, particularly for the samples with the highest degree of branching. A modified Cohen–Turnbull–Fujita free volume model adequately described the diffusivity data. The free volume of the penetrable phases was strongly dependent on their total volume fraction, suggesting the presence of an interfacial penetrable component with low fractional free volume. The dependence of the fractional free volume of the penetrable phases on the phase composition suggests that mass transport takes place from the liquid-like component to the interfacial component and that the penetrant molecules are trapped at the interfacial sites. The decrease in geometrical impedance factor with increasing crystallinity may be explained by the presence of extraordinarily wide dominant crystal lamellae in the heterogeneous low crystallinity samples. The saturation concentration of *n*-hexane in a wide range of polyethylenes (including the heterogeneous poly(ethylene-*co*-octene)s, linear polyethylenes and poly(ethylene-*co*-butene)s reported earlier; crystallinity range: 30–94%) showed a complex non-linear dependence on crystallinity that was qualitative in accordance with rubber elasticity theory considering also molecular cilia.

Keywords: Diffusion; Poly(ethylene-*co*-octene)s; Free volume

1. Introduction

Penetrant diffusion through polymers is greatly affected by the presence of crystallites. A crystallite is impenetrable to most of the non-reactive molecules except for the very smallest molecules such as helium [1]. The penetrant molecules have to circumvent the crystallites and thus 'travel' a much longer distance through a semicrystalline polymer than through a fully amorphous polymer. This is conveniently described by a single factor, the so-called geometrical impedance factor (τ) that is simply defined as the ratio of the diffusivity of the hypothetical fully amorphous polymer (D_a) to that of the semicrystalline polymer (D) [2]:

$$\tau = \frac{D_a}{D} \tag{1}$$

The crystallinity and the width-to-thickness ratio of the crystallites are decisive factors for the geometrical impedance factor. There have been relatively few attempts to calculate the geometrical impedance factor from morphological data and to compare these to experiments. Hedenqvist et al. [3] used the Fricke model [4] for a series of polyethylenes. Input data were crystallinity and crystal width-to-thickness data obtained by electron microscopy. Good agreement between calculated and experimental geometrical impedance factor data was obtained for linear polyethylenes with crystallinities from 50 to 94% [3].

A second factor that has to be considered in semicrystalline polymers is the constraining effect of the crystallites on the amorphous chain segments. Both the mechanical data, applying composite theory to dynamic mechanical data [5], and the transport property data [3] indicate that the segmental mobility of the non-crystalline fraction is much less than that of the fully amorphous analogue. The constraining effect was represented in the early work of Michaels and Bixler [5] by an empirical factor (β):

$$D = \frac{D_a}{\tau\beta} \tag{2}$$

Free volume theory according to Cohen and Turnbull [7,8]

* Corresponding author. Tel.: +46-8-7907640; fax.: +46-8-208856.
E-mail address: gedde@polymer.kth.se (U.W. Gedde).

0032-3861/01/$ - see front matter
PII: S0032-3861(00)00931-9

Nomenclature

A	pre-exponential factor in free volume equation
a_1	activity of the penetrant in the penetrable fraction of the polymer
A_d	constant in free volume equation
B	blocking factor
B_d	constant in free volume equation
D	diffusivity
D_{12}	diffusivity of penetrant with the polymer as a fixed reference frame
D_a	diffusivity of hypothetical amorphous polymer
D_c	concentration dependence factor of the diffusivity
$D_{c\to 0}$	zero-concentration diffusivity
D_I	diffusivity in the interfacial component(s)
D_L	diffusivity in the liquid-like component
D_T	thermodynamic diffusivity
f	fractional free volume
F_0	rate of evaporation
f_1	fractional free volume of penetrant
f_2	fractional free volume of the amorphous (penetrable) fraction of the polymer
f_2^{IL}	fractional free volume of interfacial liquid-like component
f_2^{L}	fractional free volume of liquid-like component
f_2^{i}	fractional free volume of each component (L, IL and ICC or L and IL) in the penetrable fraction of the polymer
I_x	intensity of Raman peak appearing at x cm^{-1}
L	half the thickness of the dry polymer specimen
L_c	crystal thickness
L_{cc}	projected length of the main-chain carbon–carbon bond
L_{ICC+IL}	thickness of interfacial layers (ICC + IL)
L_{IL}	thickness of interfacial liquid-like layer (IL)
LP	long period
$\bar{M}_c$	number average molar mass of amorphous chain segments
$\bar{M}_n$	number average molar mass of polymer
M_{rep}	molar mass of repeating unit of polymer
$\bar{M}_w$	weight average molar mass of polymer
SSD	sum of squares difference
t	time
w	crystal width
v_1	volume fraction of penetrant in polymer
w_c	mass crystallinity
w_{CC}	mass fraction of crystal core component in polymer
v_{CC}	volume fraction of crystal core component in polymer
w_{ICC}	mass fraction of interfacial crystal core component in polymer
v_{ICC}	volume fraction of interfacial crystal core component in polymer
v_I^n	volume fraction of interfacial component(s) in penetrable polymer fraction
v_L^n	volume fraction of liquid-like component in penetrable polymer fraction
v_1^a	volume fraction of penetrant in amorphous (penetrable) phase
v_2^a	volume fraction of polymer in amorphous (penetrable) phase
V_1^0	molar volume of penetrant
w_{IL}	mass fraction of interfacial liquid-like component in dry polymer
v_{IL}	volume fraction of interfacial liquid-like component in dry polymer
w_L	mass fraction of liquid-like component in dry polymer
v_L	volume fraction of liquid-like component in dry polymer
x	depth position in film specimen
Greeks	
β	empirical factor that reduces diffusivity due to the constraining effect of crystals
χ_{12}	Flory–Huggins interaction parameter
ϕ	mass fraction of penetrable phases
ρ_1	density of penetrant
ρ_2	density of polymer
ρ_a	density of amorphous fraction of polymer
ρ_c	density of crystalline fraction of polymer
ρ_{CC}	density of crystal core component
ρ_{ICC}	density of interfacial crystal core component
ρ_{IL}	density of interfacial liquid-like component
ρ_L	density of liquid-like component
τ	geometrical impedance factor
ψ	detour factor

and Fujita [9] was used by Hedenqvist et al. [3] to describe the *n*-hexane desorption from a series of polyethylenes with different crystallinities and morphologies. A simple formulation of the free volume theory is:

$$D \propto \exp(-(B_d/f)) \tag{3}$$

where f is the fractional free volume and B_d is a constant that depends only on the size of the penetrant molecule [10]. For a semicrystalline polymer through which diffusion occurs in the amorphous component, it is possible to combine the free volume theory and the empirical formulation of the geometrical impedance factor in a single equation:

$$D = \left(\frac{\psi}{B}\right) RTA_d \exp(-(B_d/f_2)) \tag{4}$$

where ψ is the detour factor, B is the blocking factor (both the concepts were introduced by Peterlin [11]), A_d is a temperature-independent constant that depends on the size

and shape of the penetrant molecule [10] and f_2 is the fractional free volume of the amorphous fraction of the polymer. The geometrical impedance factor is readily identified as:

$$\tau = \frac{B}{\psi} \tag{5}$$

and the constrained amorphous diffusivity (D_a/β) is:

$$\frac{D_a}{\beta} = RTA_d \exp(-(B_d/f_2)) \tag{6}$$

It is not possible to obtain the values for each individual pre-exponential factor in Eq. (4) by analysis of isothermal desorption data. Hence, these factors are brought together in a single parameter (A):

$$D = A \exp(-(B_d/f_2)) \tag{7}$$

Note that A is inversely proportional to the geometrical impedance factor (τ). This equation is applicable to the diffusion of penetrants that do not change the free volume of the system. If the penetrant brings additional free volume to the amorphous fraction, this can be conveniently described by considering the free volume of the amorphous fraction as the sum of the contributions from the amorphous fraction of the polymer and the penetrant [12]:

$$D = A \exp(-(B_d/(v_1^a f_1 + v_2^a f_2))) \tag{8}$$

where $v_1^a + v_2^a = 1$ (v_1^a and v_2^a are, respectively, the volume fractions of penetrant and polymer in the amorphous fraction), f_1 is the fractional free volume of the pure penetrant and f_2 is the fractional free volume of the amorphous fraction of the pure polymer. Eq. (8) is valid only for systems which exhibit a constant volume on mixing. Eq. (8) implies that D increases with increasing concentration of penetrant when $f_1 > f_2$. Eq. (8) can be rewritten in order to separate the zero-concentration diffusivity ($D_{c\to 0}$) and the penetrant–concentration-dependence (D_c) into different factors [3]:

$$D = A \exp(-(B_d/f_2)) \times \exp((B_d v_1^a (f_1 - f_2))/(f_2(f_2 + v_1^a(f_1 - f_2)))) = D_{c\to 0} D_c \tag{9}$$

Fleisher [12] and Hedenqvist et al. [3] showed for desorption data taken for a series of polyethylenes that f_2 depended on the crystallinity and, furthermore, it was considerably smaller than that of a fully amorphous analogue. Inspired by the Strobl model [13,14], which is based on Raman spectroscopy data, it was proposed by Hedenqvist et al. [3] that the non-crystalline fraction of polyethylene consists of a liquid-like component that resembles the fully amorphous polymer and a constrained component with reduced segmental mobility and lower effective free volume (interfacial component). Analysis of desorption data suggested that the fractional free volume of the interfacial component was considerably lower than the 8–9% of the liquid-like component [3]. The excellent agreement between experimental and fitted desorption data, and the realistic crystallinity dependence of the geometrical impedance factor were strong arguments supporting the validity of this free volume approach. Desorption data for poly(ethylene-*co*-butene)s with crystallinities ≥45% could be described by Eq. (9) and realistic free volumes were obtained [3]. However, the data for the geometrical impedance factor obtained by the fitting decreased with increasing crystallinity, which seemed physically unrealistic.

This paper presents *n*-hexane desorption data for heterogeneous poly(ethylene-*co*-octene)s with even lower mass crystallinities (≥30%) than those tested before, and the free volume theory is critically tested. The term 'heterogeneous' refers to the fact that the comonomers are unevenly distributed among different molecules; the low molar mass species are more branched on an average. In addition, at each chain length, molecules exist with few and many branches. The heterogeneity results from the use of a catalyst having atleast two active sites. Different numerical methods have been tried to make the results physically realistic. The experimental data are evaluated together with earlier reported data [3] for other polyethylenes in an attempt to attain a unified description for all polyethylenes. The samples with the lowest degree of crystallinity contained very small crystallites that are not included in the crystal core component as revealed by Raman spectroscopy. It is highly relevant to ask what part of the structure is penetrable by *n*-hexane in the diffusion process. A comparison is also made between Raman data, classical crystallinity assessments using density measurements, differential scanning calorimetry and X-ray scattering and data for the interfacial component obtained by small-angle X-ray scattering and proton nuclear magnetic resonance spectroscopy.

2. Experimental

Molecular structure data and the densities of the polymers studied are presented in Table 1. All these polymers were heterogeneous poly(ethylene-*co*-octene)s prepared by using Ziegler–Natta catalysts according to procedures described elsewhere [15]. Circular sheets, 1 mm thick and with a diameter of 61 mm, were made by compression moulding at 453.2 K for 10 min followed by 0.3 K min^{-1} cooling to 300 K while the pressure was maintained using a Schwabenthan Polystat 400s compression-moulding machine.

Before desorption, the sheets were immersed in liquid *n*-hexane (purity 99%; Merck; density $\rho_1 = 656$ kg m^{-3} at 298.2 K) at 298.2 K until sorption equilibrium was attained. The saturated sheets were then exposed to air at 298.2 K and the desorption kinetics were monitored by intermittent weighing of the samples on a Mettler AE balance. With the exception of sample S8, the loss of polymer material into the *n*-hexane liquid during sorption was low: <1 wt.% for S1–S6, <2 wt.% for S7 and <25 wt.% for sample S8.

The densities (ρ_2) at 298.2 K of the materials were

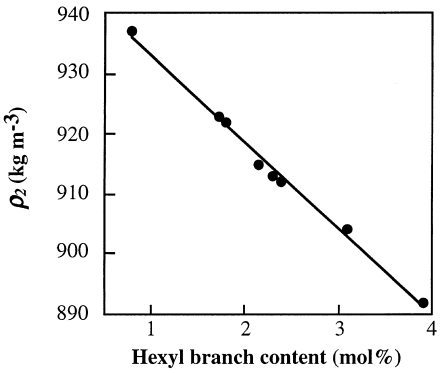

Fig. 1. Density at 298 K (ρ_2) as a function of the hexyl-branch content as determined by infrared spectroscopy.

determined using the Archimedean principle, i.e. by weighing the specimens in air and in ethanol (density = 790 kg m^3 at 298.2 K). A top-loaded Mettler AE balance with pan diameters of 80 and 130 mm equipped with the Kit ME-33360 was used.

Raman spectra were recorded at 300 K using a Perkin–Elmer Spectrum 2000 NIR-Raman instrument. Each spectrum was based on 256 scans. The runs were interrupted after 128 scans in order to limit the temperature rise of the specimens. Two sheets were placed together in order to increase the Raman intensity-to-noise ratio.

3. Theory and parameter determination

Fick's second law of diffusion for a sheet can be written as:

$$\frac{\partial v_1}{\partial t} = \frac{\partial}{\partial x}\left(\frac{D_{12}}{(1-v_1)}\frac{\partial v_1}{\partial x}\right) \tag{10}$$

where D_{12} is the diffusivity of the penetrant, with the polymer as the fixed reference frame (subscripts 1 and 2 refers to the penetrant and polymer, respectively) [9], v_1 is the volume fraction of penetrant dissolved in the polymer at time t and position x. D_{12} is related to the thermodynamic diffusivity D_T through [9]:

$$\frac{D_{12}}{(1-v_1)} = D_T\left(\frac{\partial \ln a_1}{\partial \ln v_1^a}\right) \tag{11}$$

where a_1 is the penetrant activity in the polymer.

Using the Flory–Huggins theory, Fels and Huang [16] showed that the activity of the penetrant absorbed in the non-crystalline part of the polymer is given by:

$$\frac{\partial \ln a_1}{\partial \ln v_1^a} = (1-v_1^a)(1-2\chi_{12}v_1^a) \tag{12}$$

where χ_{12} is the Flory–Huggins interaction parameter, which for PE/*n*-hexane takes values between 0.7 and 1.0 depending on the *n*-hexane concentration [17]. The *n*-hexane-concentration-dependence of χ_{12} reported by Rogers et al. [17] was used in the calculations. It was also found that the precise value used for χ_{12} had only a very small effect on the results of the fittings, i.e. on the fitted values for the adjustable parameters A and f_2. A similar conclusion was drawn by Fels and Huang [16]. Eqs. (10)–(12) may be combined to give the expression:

$$\frac{\partial v_1}{\partial t} = \frac{\partial}{\partial x}\left[D_T(1-v_1^a)(1-2\chi_{12}v_1^a)\frac{\partial v_1}{\partial x}\right] \tag{13}$$

The thermodynamic diffusivity (D_T) was expressed according to the free volume theory assuming constant mixing volume (see Section 1, Eq. (9)):

$$D_T = A\exp(-(B_d/f_2)) \times \exp((B_d v_1^a(f_1-f_2))/(f_2(f_2+v_1^a(f_1-f_2)))) = D_{c\to 0}D_c \tag{14}$$

The unknown, adjustable parameters were obtained by numerical solution of Eqs. (13) and (14) using the following outer and inner boundary conditions:

$$D_T(1-v_1^a)(1-2\chi_{12}v_1^a)\left(\frac{\partial v_1}{\partial x}\right)_{x=0} = F_0 v_1 \tag{15}$$

$$\left(\frac{\partial v_1}{\partial x}\right)_{x=L} = 0 \tag{16}$$

where x is the distance from the surface of the sheet; the thickness of the sheet is $2L$. The rate of evaporation (F_0) was determined according to the method proposed by Bakhouya et al. [18]. The parameter B_d was set to 0.8 [12]. Further details about the numerical methods in the calculation can be found in Refs. [3,19,20].

In the numerical calculations, six different methods were used and the results obtained were compared. Both the goodness of fit and the physical realism of the results were considered. The methods were as follows:

(i) The penetrable phases were interfacial crystal core (ICC), interfacial liquid-like (IL) and liquid-like (L) components; further details about these components are presented in Section 4.1, $f_1 = 0.168$ [12], A and f_2 were the adjustable parameters.
(ii) The penetrable phases were IL and L components,

Table 1
Molecular structure of polymers studied

Sample code	$\bar{M}_w$ [a] (g mol^{-1})	$\bar{M}_w/\bar{M}_n$ [a]	Density (kg m^{-3})	X_{hex} [b]
S1	88 000	5.2	937	0.78
S2	107 500	4.6	923	1.72
S3	79 000	4.0	922	1.80
S4	88 000	3.8	915	2.14
S5	110 000	4.1	913	2.30
S6	81 000	4.7	912	2.38
S7	95 000	4.3	904	3.09
S8	87 000	5.8	892	3.91

[a] By size exclusion chromatography.
[b] Mole per cent of hexyl branches by IR spectroscopy.

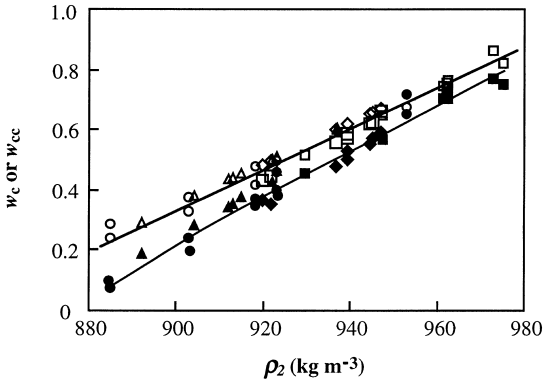

Fig. 2. Mass crystallinity (w_c or w_{CC}) by several methods as a function of density at 298 K (ρ_2). By Raman spectroscopy (CC component): ▲ heterogeneous poly(ethylene-*co*-octene)s (S samples); ● poly(ethylene-*co*-octene)s (metallocene-based technology) and LDPE, from Lagarón et al. [22]; ◆ poly(ethylene-*co*-butene)s, from Hedenqvist et al. [3]; ■ linear polyethylenes, from Hedenqvist et al. [3]. By conventional techniques: △ heterogeneous poly(ethylene-*co*-octene)s, by density measurements; ○ poly(ethylene-*co*-octene)s (metallocene-based technology) and LDPE, by X-ray scattering and DSC, from Lagarón et al. [22]; ◇ poly(ethylene-*co*-butene)s, by DSC and density measurements, from Hedenqvist et al. [3]; □ linear polyethylenes, by DSC and density measurements, from Hedenqvist et al. [3].

$f_1 = 0.168$ [12], A and f_2 were the adjustable parameters.
(iii) The penetrable phases were ICC, IL and L components, $f_1 = 0.168$ [12], A was constrained to a value prescribed by the Fricke model according to data from Hadgett et al. [21], assuming a constant crystal width-to-thickness ratio of 35, only f_2 was the adjustable parameter.
(iv) The penetrable phases were IL and L components, $f_1 = 0.168$ [12]; A was constrained to a value prescribed by the Fricke model according to data from Hadgett et al. [21], assuming a constant crystal width-to-thickness ratio of 35; only f_2 was the adjustable parameter.
(v) The penetrable phases were ICC, IL and L components, A was constrained to a value prescribed by the Fricke model according to data from Hadgett et al. [21], assuming a constant crystal width-to-thickness ratio of 35; f_1 and f_2 were the adjustable parameters.
(vi) The penetrable phases were IL and L components; A was constrained to a value prescribed by the Fricke model according to data from Hadgett et al. [21], assuming a constant crystal width-to-thickness ratio of 35; f_1 and f_2 were the adjustable parameters.

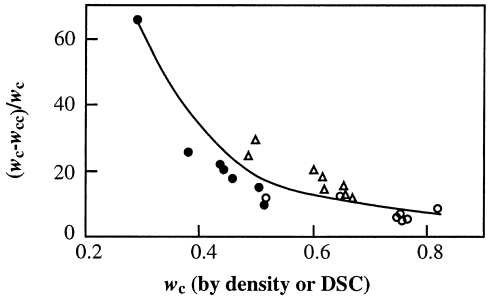

Fig. 3. Difference between crystallinity by DSC or density (w_C) and crystal core content (w_{CC}) by Raman normalised with respect to w_C as a function w_C: ● heterogeneous poly(ethylene-*co*-octene)s; △ poly(ethylene-*co*-butene)s, from Hedenqvist et al. [3]; ○ linear polyethylenes, from Hedenqvist et al. [3].

4. Results and discussion

4.1. Crystallinity and phase composition

Fig. 1 shows that the density of the heterogeneous poly(-ethylene-*co*-octene)s was proportional to the hexyl-branch-content. Mass crystallinity (w_C) was obtained from density data (ρ_2), according to:

$$w_C = \frac{(1/\rho_2) - (1/\rho_a)}{(1/\rho_c) - (1/\rho_a)} \tag{17}$$

where $\rho_c = 1000$ kg m^{-3} [22] and $\rho_a = 855$ kg m^{-3} [22] are the crystal and amorphous densities at 298.2 K. The crystallinities obtained from density measurements are presented in Table 2.

Raman spectra were analysed according to Mutter, Stille and Strobl [14] as described by Hedenqvist et al. [3]. Mass contents of the orthorhombic crystal core component (CC), the liquid-like amorphous component (L) and the two interfacial components (ICC: chain sections in all-*trans* conformation without regular orthorhombic packing and IL: chains with modified conformation, higher *trans* content than that of the unconstrained liquid) were obtained from the intensities of the CH_2-rocking (700–970 cm^{-1}); CH_2-twisting (1250–1350 cm^{-1}) and CH_2-bending (1390–1510 cm^{-1}) regions of the Raman spectrum [13,14]. Hexacontane was used as a 100% CC standard and *n*-octadecane as a 100% L standard. Overlapping peaks were resolved by fitting a series of Lorentz functions to the experimental data according to Hedenqvist et al. [3].

The mass fractions of the four components were obtained by taking the resolved intensities (I_x) of the different bands

Table 2
Mass crystallinity and mass fractions of components as revealed by Raman spectroscopy

Sample code	w_D[a]	w_{CC}[b]	w_{ICC}[b]	w_{IL}[b]	w_L[b]
S1	0.607	0.601	0.037	0.158	0.204
S2	0.514	0.464	0.069	0.151	0.316
S3	0.505	0.430	0.090	0.158	0.322
S4	0.457	0.375	0.115	0.170	0.340
S5	0.443	0.352	0.116	0.173	0.359
S6	0.437	0.341	0.120	0.176	0.363
S7	0.379	0.281	0.108	0.184	0.427
S8	0.290	0.190	0.104	0.178	0.528

[a] From density data (s.d. ±0.015).
[b] From Raman spectra (s.d.: ±0.015).

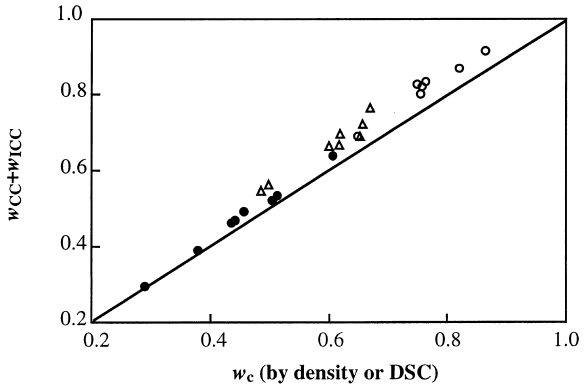

Fig. 4. Crystal core content (w_{CC}) and content of ICC component (w_{ICC}) as a function of crystallinity by DSC or density measurements (w_c): ● heterogeneous poly(ethylene-*co*-octene)s; △ poly(ethylene-*co*-butene)s, from Hedenqvist et al. [3]; ○ linear polyethylenes, from Hedenqvist et al. [3].

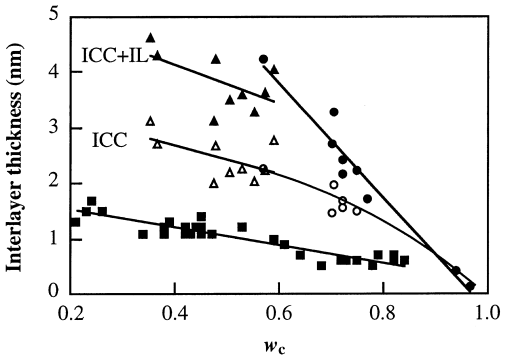

Fig. 5. Thickness of interlayer as a function of mass crystallinity (w_c) calculated from Eq. (22) using Raman data from Ref. [3]: ● linear polyethylenes and ▲ poly(ethylene-*co*-butene)s and from Eq. (23) using data from the same source: ○ linear polyethylenes and △ poly(ethylene-*co*-butene)s. Data based on small-angle X-ray scattering from Vonk and Pijpers [24] are presented [symbol: ■] in the same diagram.

according to:

$$w_{CC} = \left(\frac{I_{1417}}{I_{(1250-1350)}}\right)\left(\frac{I_{1417}}{I_{(1250-1350)}}\right)^{-1}_{w_{CC}=1} \tag{18}$$

$$w_L = \left(\frac{I_{(700-970)}}{I_{(1250-1350)}}\right)\left(\frac{I_{(700-970)}}{I_{(1250-1350)}}\right)^{-1}_{w_L=1} \tag{19}$$

$$w_{IL} = \frac{I_{1303}}{I_{(1250-1350)}} - w_L \tag{20}$$

$$w_{ICC} = 1 - w_{CC} - w_L - w_{IL} \tag{21}$$

Table 2 presents a summary of the mass fractions of the four components together with the density-based crystallinity for all samples. Fig. 2 shows that the crystal-core mass fraction (w_{CC}) is lower than the density-based crystallinity particularly at lower densities (crystallinities). Fig. 2 also shows that the data agree with the recent data of Lagarón et al. [23], who proposed that a fraction of the crystals have defects and a critical drop in crystalline density. The fraction of defective crystals increases with decreasing overall density and it is not accounted for in the CC component by Raman spectroscopy. Martinez-Salazar [24] found that highly branched polyethylene showed, in addition to the orthorhombic crystals, a significant fraction of a crystal phase with hexagonal packing. The latter is not included in the Raman CC-component. The difference between w_C and w_{CC} was relatively small for the polyethylenes with higher crystallinities: 0.055 for linear polyethylenes [3], which was on an average 8% of the crystalline content. For poly(ethylene-*co*-butene)s, the difference was 0.107 [3], which was on an average 18% of the crystalline content. The corresponding values for the heterogeneous poly(ethylene-*co*-octene)s were 0.085 and 22%.

Fig. 3 shows the difference between w_C (by density or DSC) and w_{CC}, normalised with reference to w_C (this quantity will be referred to as Δ) as a function of w_C. Highly crystalline linear polyethylenes show relatively small Δ values, less than 10% at crystallinities above 70%. There is a considerable variation in the data for the branched polyethylenes; the poly(ethylene-*co*-butene)s show larger Δ values than the poly(ethylene-*co*-octene)s at the same crystallinity. The overall trend in the data is however clear, namely that Δ increases with decreasing crystallinity. The sample with the lowest degree of crystallinity ($w_C \approx 30\%$) shows a Δ value close to 65%. It may be argued that it is rather the crystal thickness that is the important factor. The linear polyethylenes, for which the average crystal thickness was constant within 10% (20 ± 2 nm) [3], showed only a minor variation in Δ as a function of crystallinity (Fig. 3). The poly(ethylene-*co*-butene)s with a crystallinity of 50% have crystals which are roughly 10 nm in thickness [3], and it is interesting to note that the Δ values for these polymers are twice that of the linear polyethylenes. It is thus suggested that a packing disorder of *trans* chains is characteristic of the crystal surfaces and that this disorder,

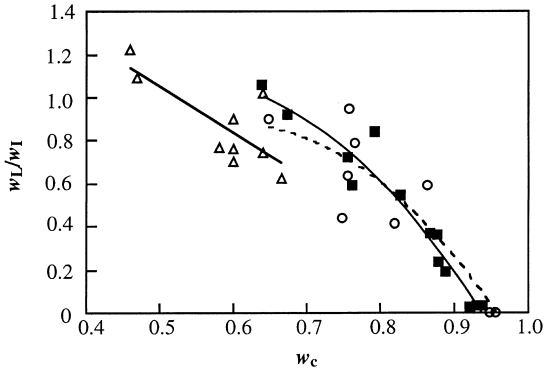

Fig. 6. Ratio of mass fractions of liquid-like to interfacial components (w_L/w_I) as a function of mass crystallinity (w_c): ■ by proton NMR, drawn from Kitamaru et al. [25]; ○ linear polyethylenes, calculated from Raman spectroscopy data of Ref. [3]; △ poly(ethylene-*co*-butene)s, calculated from Raman spectroscopy data of Ref. [3].

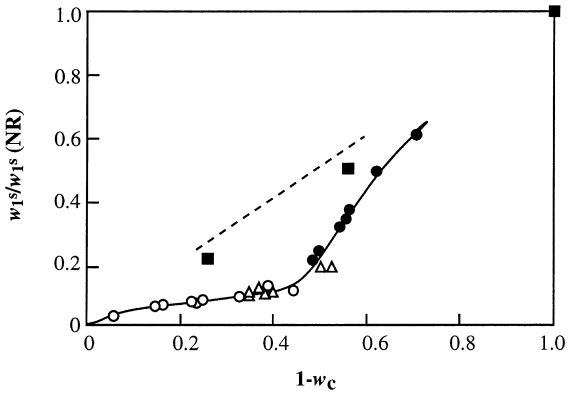

Fig. 7. Saturation concentration of *n*-hexane (w_1^s) as a function of the amorphous content ($1 - w_c$) from density: ● heterogeneous poly(ethylene-*co*-octene)s; △ poly(ethylene-*co*-butene)s, from Hedenqvist et al. [3]; ○ linear polyethylenes, from Hedenqvist et al. [3]. The data are normalised with respect to the solubility of *n*-hexane in natural rubber (NR; $\bar{M}_c \approx 2500$ g mol^{-1}), ~0.56 kg *n*-hexane/kg total. The solubilities of oxygen in LDPE, HDPE and NR (denoted ■; data from Michaels and Bixler [6]) are also shown.

evident by Raman spectroscopy in the smaller crystal core content, is most evident for the highly branched polymers with their thin crystals. Fig. 4 shows a comparison between DSC/density crystallinity and Raman data including both the crystal core and the ICC. For the heterogeneous poly(ethylene-*co*-octene)s there is a good agreement between these quantities for the two samples of lowest crystallinity. The other six poly(ethylene-*co*-octene)s of higher crystallinity showed slightly higher $w_{CC} + w_{ICC}$ than w_C, by 0.03–0.05. Less branched and linear polyethylenes showed a larger difference between $w_{CC} + w_{ICC}$ and w_C, 0.05–0.10.

It is interesting to make further comparisons between the Raman data and data obtained by small-angle X-ray scattering (SAXS) on the thickness of the interlayer (the region where the density changes from the crystal to the liquid value) and by proton NMR probing the segmental mobility. Fig. 5 shows data for the interlayer thickness from Vonk and Pijpers [25] compared with data calculated from Raman data reported by Hedenqvist et al. [3]. The thickness of the ICC + IL layer was calculated according to the following expressions:

$$L_{ICC+IL} = \frac{LP}{2}\left[\frac{(w_{ICC} + w_{IL})/\rho_I}{(w_{ICC} + w_{IL})/\rho_I + w_{CC}/\rho_{CC} + w_L/\rho_L}\right] \quad (22)$$

$$L_{ICC} = \frac{LP}{2}\left[\frac{w_{ICC}/\rho_I}{(w_{ICC} + w_{IL})/\rho_I + w_{CC}/\rho_{CC} + w_L/\rho_L}\right] \quad (23)$$

where LP is the long period, $\rho_I \approx 900$ kg/m^3 [3] is the density of the interfacial components, $\rho_{CC} = 1000$ kg m^{-3} [22] is the crystal density and $\rho_L = 855$ kg m^{-3} [22] is the density of the liquid-like component. Fig. 5 shows clearly that the thickness of the density gradient (SAXS) is considerably sharper than the thickness of ICC and ICC + IL. However, the thickness of the IL component (the difference between the ICC + IL and ICC curves) shows approximately the same crystallinity-dependence as the interlayer thickness as determined by SAXS (Fig. 5).

A comparison between the NMR data reported by Kitamaru et al. [26] using the method of Bergmann and Nawatki [27–29] and the Raman data from Hedenqvist et al. [3] is shown in Fig. 6. The proton NMR method used by Katamaru et al. [26] probes segmental mobility and three components are defined: orthorhombic crystalline, liquid-like amorphous (L) and a component of intermediate segmental mobility (I). The ratio of the mass fraction of the liquid-like amorphous component to that of the intermediate component based on NMR data shows a crystallinity dependence very similar to that of the liquid-like and the interfacial components ($w_{ICC} + w_{IL}$) based on Raman spectroscopy (Fig. 6).

4.2. Solubility

Fig. 7 shows the crystallinity dependence of the saturation concentration of *n*-hexane for a series of polyethylenes, including the heterogeneous poly(ethylene-*co*-octene)s (S1–S8), the linear polyethylenes and the poly(ethylene-*co*-butene)s earlier reported by Hedenqvist et al. [3]. The complex curve shape itself indicates that several factors are important. The data for the oxygen solubility may serve as a good starting point for discussion. The oxygen solubility is essentially proportional to the fraction of amorphous component, which confirms that oxygen only penetrates into the amorphous fraction of the polymer. Another important piece of information is that the solubility of oxygen at these low partial pressures is low and there is essentially no change in the volume of the polymer.

The swelling caused by the uptake of *n*-hexane by the low crystallinity samples (S7 and S8) was extensive, close to 30% for these particular samples. The strong increase in solubility with increasing amorphous content (w_a) for samples with $w_a \geq 0.4$ must be due to the increase in length of the amorphous chain segments with decreasing crystallinity. These polymers show a resemblance to thermoplastic elastomers with the crystals acting as physical crosslinks and the amorphous chain segments stretching out in the presence of the solvent. The equilibrium degree of swelling for an affine network is given by [30]:

$$\ln v_1 + (1 - v_1) + \chi_{12}(1 - v_1)^2 = -\frac{\rho_2}{\bar{M}_c} V_1^0 (1 - v_1)^{1/3} \quad (24)$$

where V_1^0 is the molar volume of the penetrant and $\bar{M}_c$ is the number average molar mass of the amorphous chain segments. The confinement of the penetrant molecules to the non-crystalline fraction of the polymer can be considered by replacing v_1 by v_1^a in Eq. (24). The 'effective' molar mass of the amorphous chain segment is calculated from Eq. (24) by inserting the appropriate value for the interaction parameter. If it is assumed that the amorphous chain segments are bridging the gap between two adjacent crystals, the thickness of the amorphous interlayer (L_a) may be calculated by assuming that the

Table 3
Free volume parameters obtained by fitting according to methods I and II

Sample	Method I				Method II			
	f_2	A	$D_{c\to 0}$[a]	SSD[b]	f_2	A	$^{D}_{c\to 0}$[a]	SSD[b]
S1	0.0490	0.0317	2.57	0.0032	0.0499	0.0216	2.36	0.0034
S2	0.0519	0.0241	4.85	0.0030	0.0522	0.0184	4.06	0.0038
S3	0.0531	0.0182	5.25	0.0012	0.0547	0.0109	4.88	0.0016
S4	0.0574	0.0101	9.04	0.0005	0.0582	0.0071	7.61	0.0003
S5	0.0594	0.0092	13.10	0.0016	0.0600	0.0069	11.20	0.0011
S6	0.0598	0.0081	12.40	0.0008	0.0600	0.0063	10.30	0.0005
S7	0.0620	0.0073	18.10	0.0013	0.0628	0.0058	16.80	0.0008
S8	0.0695	0.0058	58.10	0.0016	0.0701	0.0053	58.60	0.0016

[a] In 10^{-9} cm^2 s^{-1}.
[b] The sum of squares difference between experimental and fitted desorption data.

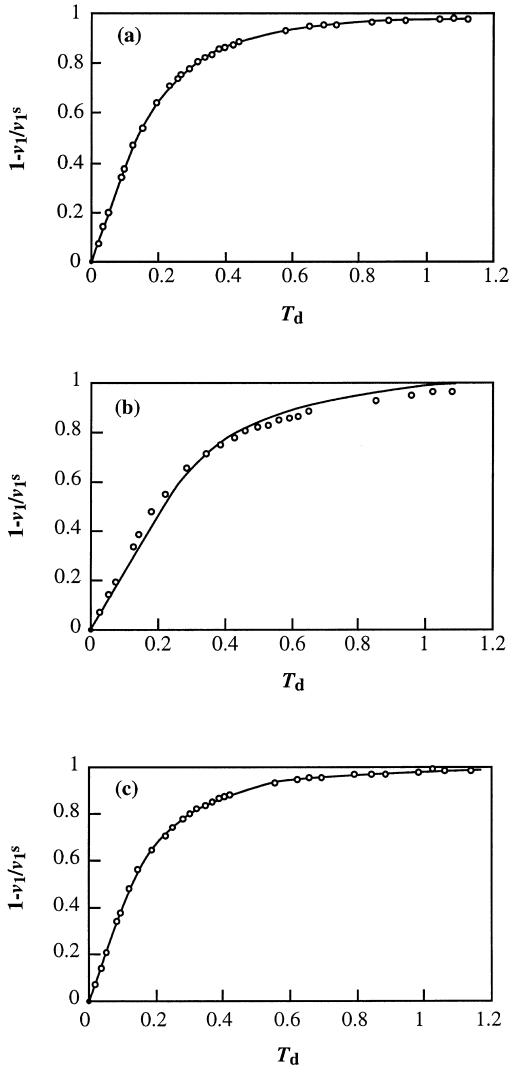

Fig. 8. Normalised *n*-hexane desorption curves for sample S4 showing experimental data (points) and fitted data (lines) according to methods I (graph a), III (graph b) and V (graph c). Dimensionless time (T_d) is defined according to $T_d = (D_{c\to 0}t/L^2)^{1/2}$, where t is time and L is half the specimen thickness. The penetrant concentration (v_1) is normalised with respect to the saturation concentration (v_1^s).

amorphous chain segments follow Gaussian statistics, viz.:

$$L_a = \sqrt{6.7 L_{cc}^2 \bar{M}_c / M_{rpu}} \quad (25)$$

where L_{cc} is the projected length of the main chain carbon–carbon bond (≈ 0.13 nm) and M_{rpu} is the molar mass of the repeating unit (≈ 14 g mol^{-1}). The factor 6.7 is the characteristic ratio of linear polyethylene at 413 K [31]. The hexyl-branched polyethylene samples showed a change in $\bar{M}_c$ from 400–600 (S1) to 11 000 g mol^{-1} (S7 and S8), which corresponds to an increase in L_a from ~2 (S1) to ~10 nm (S7 and S8). The values are quite sensitive to the actual value chosen for the interaction parameter, 0.7–1.0 [17]. The five-fold change in L_a is not consistent with the two-fold change calculated from melting point data (revealing crystal thickness via the Gibbs–Thomson equation) and crystallinity data for these particular samples. However, the length of the amorphous chain segments for sample S1 may be so small that it violates the Gaussian approximation of the rubber elasticity theory as expressed in Eq. (24).

Another complicating effect arises from the complex morphology of the heterogeneous poly(ethylene-*co*-octene)s with a phase separation between molecules of different degrees of branching [32]. In S7 the least branched molecules are space filling and the most branched molecules separate in a disperse phase. In S8 the most branched molecules constitute the matrix whereas the least branched molecules form connected compact semicrystalline domains leading to a co-continuous morphology [32].

The rubber elastic character of these polymers as expressed by Eqs. (24) and (25) cannot alone explain the low increase in solubility with increasing amorphous content found for the linear polyethylenes. Cilia will not contribute to the swelling forces and hence solubility is favoured by the presence of chain ends. The weakness of the change in solubility over this wide crystallinity range is thus due to two counteracting effects: the decrease in number of cilia and the increase in length of the amorphous chain segments with increasing molar mass (and decreasing

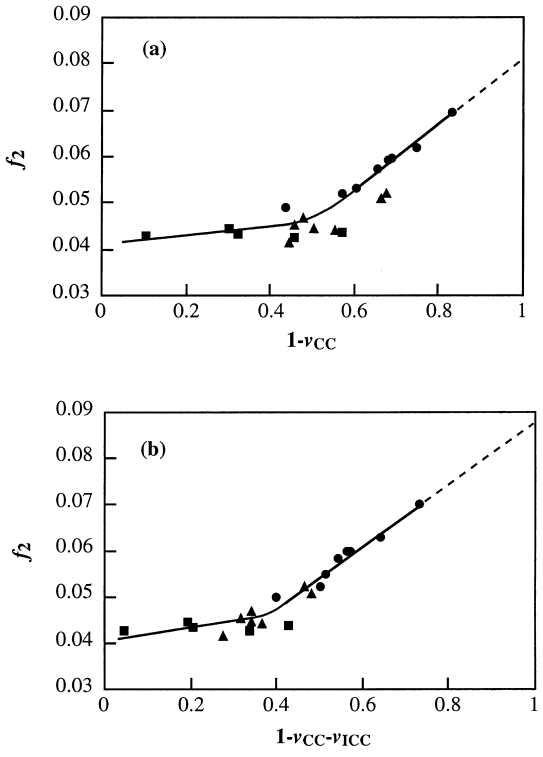

Fig. 9. Fractional free volume of penetrable fraction of polymer (f_2) as a function of fraction of penetrable polymer: graph (a) f_2 calculated according to method I; graph (b) f_2 calculated according to method II ● heterogeneous poly(ethylene-*co*-octene)s; ▲ poly(ethylene-*co*-butene)s, from Hedenqvist et al. [3]; ■ linear polyethylenes, from Hedenqvist et al. [3].

crystallinity). The first of the two leads to a decrease and the second to an increase in the solubility.

4.3. Desorption data; fitting of the free volume equation

The concentration of *n*-hexane in the penetrable phases (v_1^a) was calculated according to:

$$v_1^a = \frac{v_1}{v_1 + \left(1 - \sum_{i=\text{CC or CC+ICC}} v_i\right)(1 - v_1)} \quad (26)$$

where v_1 is the volume fraction of penetrant in the polymer–penetrant system ($v_1 + v_2 = 1$), $\sum_{i=\text{CC or CC+ICC}} v_i$ is the volume fraction of non-penetrable phases (CC in the case of methods I, III and IV; CC + ICC in the case of methods II, IV and VI) in the penetrant-free polymer ($v_{CC} + v_{ICC} + v_{IL} + v_L = 1$). In the conversion from mass to volume fractions the following density values were used: $\rho_{CC} = 1000$ kg m^{-3} [22], $\rho_L = 855$ kg m^{-3} [22] and $\rho_{ICC} = 930$ kg m^{-3}. The latter is estimated from data of Hedenqvist et al. [3] and data presented in this paper. The results of the fittings according to methods I and II are shown in Table 3. The sum of squares difference (SSD) between fitted and experimental data are very similar in both cases: SSD = 0.00165 (method I: L, IL and ICC are the penetrable phases) and SSD = 0.00164 (method II: L and IL are the penetrable phases). Fig. 8a shows the excellent agreement between experimental and fitted data, which was a characteristic feature of all samples and both methods.

The fractional free volume values of the penetrable polymer were also very similar, the value obtained for method II being 0.0007 larger than that obtained by method I. The pre-exponential factor (A) obtained, which is inversely proportional to the geometrical impedance factor (τ), was larger for method I than for method II, particularly for the samples with higher crystallinity. Both methods yield an increase in A with increasing crystallinity (cf. Tables 2 and 3). According to the results obtained by methods I and II, τ decreases with increasing crystallinity. This unexpected trend is consistent with earlier findings reported for poly(ethylene-*co*-butene)s [3].

The apparently physically unrealistic feature of one of the adjustable parameters obtained by methods I and II was addressed by methods III and IV. The parameter A was here constrained to values prescribed by the Fricke model assuming a universal crystal width-to-thickness ratio of 35 for all samples and f_2 was the only adjustable parameter in the fitting. These methods were not successful; the average SSD:s were 0.069 (method III) and 0.080 (method IV) which are 40–50 times greater than the SSD:s obtained from methods I and II. The poor result of the fit in the case of methods III and IV is further demonstrated in Fig. 8b.

It was possible to fit the equations with constrained A parameter values using methods V and VI. The goodness of fit, expressed as SSD, was very similar to that obtained by methods I and II, which is also shown in Fig. 8c. One of the adjustable parameters, the fractional free volume of the penetrant (f_1), showed unrealistic variation with the crystallinity, which is expressed in the following series of fitted f_1 data: 0.261 (S1), 0.210 (S4) and 0.191 (S8). These values should be compared with the value reported by Fleischer [12]: $f_1 = 0.168$.

It thus seems that none of the methods used gave satisfactory results. Good numerical results were obtained in the case of methods I, II, V and VI, but one of the adjustable parameters apparently takes physically unrealistic values in these cases. Methods III and IV are unable to fit the experimental data and they can be discarded. The extensive variation in fractional free volume of the penetrant violates the basis of the free volume theory, and methods V and VI can be discarded.

Let us examine the results obtained by methods I and II. The four- to five-fold increase in A over the crystallinity range 30–60% is unexpected and the question is whether it is an artefact indicating a serious flaw in the free volume approach or whether it can be given a morphological explanation. The results indicate that the geometrical impedance factor (τ) decreases with increasing crystallinity. Both the Fricke model [4] and the results reported by Hadgett et al. [21] from three-dimensional lattice modelling show that both the degree of crystallinity and the shape of the crystals are decisive factors for τ; at constant crystal shape

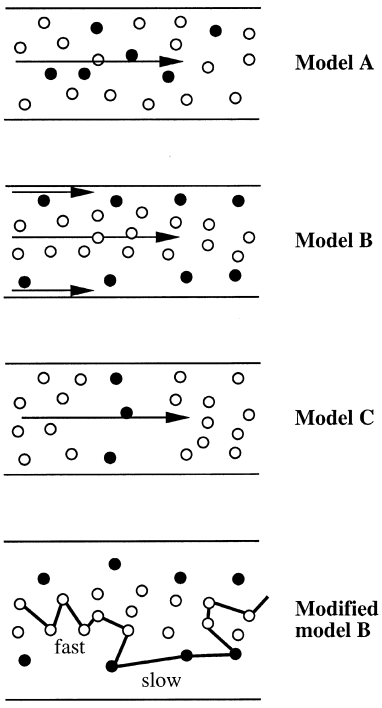

Fig. 10. Schematic representation of different models of the penetrable phase between two crystal lamellae. Unfilled circles represent the liquid-like component. The filled circles represent the interfacial component.

anisotropy, τ increases with increasing crystallinity, at constant crystallinity: τ increases with increasing crystal shape anisotropy. It may be instructive to start with narrow fractions of linear polyethylene. Linear polyethylenes showed an increase in crystal width-to-thickness (w/L_c) ratio from 18 ($w_c = 51\%$; $\bar{M}_w = 1\,040\,000$ g mol^{-1}) to 60 ($w_c = 76\%$; $\bar{M}_w = 29\,000$ g mol^{-1}) with increasing crystallinity [3]. The average crystal thickness of the linear polyethylenes was almost constant and consequently the width of the crystals and the average thickness of the amorphous layers changed as a function of crystallinity [3]. The results of the fitting of the free volume equation (method I) indicated that τ increased with increasing crystallinity [3]. A more precise analysis of the morphological data using the Fricke model gave results consistent with the results obtained by fitting the free volume equation [3]. The picture for the linear polyethylene fractions is thus simple: the geometrical impedance factor increases with increasing crystallinity because of the combined effect of an increase in crystallinity and an increase in crystal shape anisotropy. It is also important to note that the uniform chain structure of these polymers also resulted in a uniform crystal shape.

The morphology of heterogeneous poly(ethylene-*co*-octene)s is very different from that of linear polyethylene. Deblieck and Mathot [32] presented micrographs of a polymer very similar to S7. This polymer exhibited dominant crystal lamellae with extraordinarily high crystal shape anisotropy; $w/L_c \approx 150$. These very wide lamellae were surrounded by thinner lamellae with much smaller lateral dimensions. The large variation in crystal thickness was also reflected in the very wide melting range (210–400 K) of these polymers [32]. The heterogeneous poly(ethylene-*co*-butene)s showed only small variations in average w/L_c (30–40) at crystallinities between 43 and 66% [3]. It is thus suggested that the presence of dominant lamellae with an extraordinarily high crystal shape anisotropy in the highly branched heterogeneous systems is the reason for their high τ and is also the reason for the 'unusual' crystallinity trend of τ for the heterogeneous poly(ethylene-*co*-octene)s.

4.4. Morphological interpretation of the amorphous free volume

Fig. 9 presents data for the fractional free volume as a function of the volume fraction of penetrable phase (1-v_{CC} or 1-v_{CC}-v_{ICC} depending on the model used). The data of the heterogeneous poly(ethylene-*co*-octene)s (S1–S8) are shown together with earlier data reported by Hedenqvist et al. [3] for linear polyethylene and poly(ethylene-*co*-butene)s. The individual data points adapt well to the general trend indicated by the continuous lines in Fig. 9. The scatter in the data is greatest at roughly 50% crystallinity where the different polyethylenes overlap in crystallinity. The data obtained by method II (IL and L components are penetrable) show less scatter than those obtained by method I. The agreement between the data for poly(ethylene-*co*-octene)s and poly(ethylene-*co*-butene)s is better for method II. The fractional free volume for natural rubber (amorphous analogue to polyethylene) was determined by Hedenqvist et al. [3] to be 0.086, which is very close to the value obtained by extrapolation to 100% content of penetrable phase of the data obtained by method II. This value is also close to the calculated value, 0.075, assuming $f_2 = 0.025$ [33] at the glass transition temperature (203.2 K) [34], a liquid volume thermal expansion coefficient $= 7.34 \times 10^{-4}$ K^{-1} [35] and a glassy volume thermal expansion coefficient $= 2.01 \times 10^{-4}$ K^{-1} [36]. The f_2 data obtained by method I yielded a value for the pure liquid of ~0.08.

The linear extrapolation of the f_2 vs.$1 - v_{CC}$ ($1 - v_{CC} - v_{ICC}$) data is only valid if the following assumptions are correct: (a) the ratio $v_L/(v_L + v_I)$ is proportional to v_L and is equal to unity at $v_L = 1$, analysis of the data presented in Table 2 confirmed the validity of this assumption (b) the fractional free volume of the penetrable components is the sum of the contributions from the individual components. The latter assumption is not fulfilled (discussion below) and hence the extrapolated value of the liquid-like component (0.08–0.09) should only be considered as a rough estimate of the relative free volume of the liquid-like component.

The effective free volume of the penetrable fraction of the polymer is according to the data presented in Fig. 9, reduced with respect to that of the unconstrained liquid-like component. Let us assume that the penetrable phases (L, IL and ICC or L and IL) have unique individual fractional free

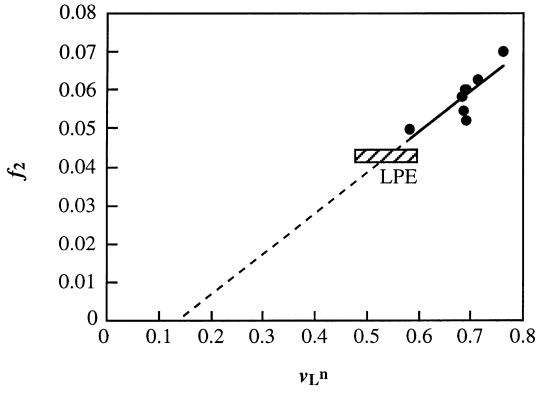

Fig. 11. Fractional free volume of the penetrable non-crystalline polymer fraction (f_2) as a function of normalised volume fraction of liquid-like component (v_L^n) for the heterogeneous poly(ethylene-*co*-octene)s. Data from Hedenqvist et al. [3] for a series of polyethylenes (LPE) are shown in the graph.

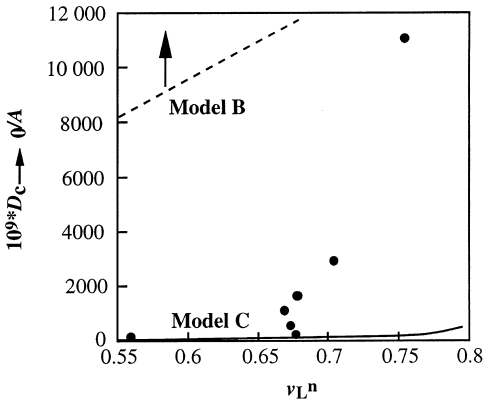

Fig. 12. Amorphous zero-concentration diffusivity (divided by A) as a function of normalised fraction of liquid-like component (v_L^n). The broken line indicates the results from model B (Eq. (29)) and the continuous line shows the results from model C (Eq. (30)).

volumes and that they contribute to the effective free volume (f_2) in relation to their volume fractions and to their location in the diffusion system. Fig. 10 shows schematically the three tested models. Model A assumes that the components are uniformly mixed (solution) in the space between the crystallites. In this case, the effective free volume of the penetrable phase is the sum of the contributions from the L and IL components, viz.:

$$f_2 = \sum_{i=\text{L,IL,ICC or L,IL}} v_i^n f_2^i \tag{27}$$

where the sum of the volume fractions is $\sum_{i=\text{L,IL,ICC or L,IL}} v_i^n = 1$. In the case of method II (L and IL are the penetrable components), Eq. (27) can be rewritten in a more suitable form for the calculation of f_2^{IL} :

$$f_2 = f_2^{IL} + v_L^n(f_2^L - f_2^{IL}) \tag{28}$$

Fig. 11 shows that a straight line in the f_2–v_L^n diagram can represent the scattered data. Data from Hedenqvist et al. [3] for linear polythylene showing a very significant variation in mass crystallinity (52–82%) but with a limited change in v_L^n (0.48–0.60) take f_2 values near 0.042 ± 0.001, which is on the regression line for the branched polymers. However, the intercept (f_2^{IL}) takes an unrealistic (negative) value. Calculations made for the other case (L, IL and ICC) give a similar result. It thus seems that model A is inconsistent with the data. Linear extrapolation of the data to $v_L^n = 1$ yields a fractional free volume for the liquid-like component of 0.092, which is close to 0.086 obtained from the extrapolation in the $f_2 - (1 - v_{CC} - v_{ICC})$ diagram (Fig. 9a).

In model B, the liquid-like and interfacial components (IL or IL + ICC) are connected in parallel in the diffusion system and the following equation holds, provided that the diffusion is independent through the two components [37]:

$$D_a = D_{c\rightarrow 0}/A = v_L^n D_L + v_I^n D_I = v_L^n(D_L - D_I) + D_I \tag{29}$$

where D_a is the free-volume-dependent part of the amorphous diffusivity, D_L is the diffusivity in the liquid component and D_I is the diffusivity of the interfacial component (IL or IL + ICC), both being divided by the A factor. The data presented in Fig. 12 clearly shows that parallel model is inconsistent with the experimental data. A series coupled diffusion system (model C) can be described by [37]:

$$\frac{1}{D_a} = \frac{v_L^n}{D_L} + \frac{1 - v_L^n}{D_I} \tag{30}$$

The diffusivities of the liquid-like and the interfacial components were calculated from the free volume equation assuming the following relative free volume values: $f_2^L = 0.08$ and $f_2^I = 0.03$. Particularly the value for f_2^I is unknown and the chosen value is just a good guess. The series-coupled model predicts too weak an increase in the diffusivity over the v_L^n range considered (Fig. 12). It is not even possible to fit the experimental data by increasing f_2^I to 0.06; the increase in diffusivity with increasing v_L^n is still too small. It must be concluded that model C is also inconsistent with the experimental data.

It can be concluded that none of the three models is a good representation of the diffusion system. Model A assumes that the constrained component is uniformly mixed with the liquid-like component. The inability of the model to yield a physically realistic relative free volume of the constrained phase is consonant with the view that this phase is located at the crystalline–amorphous interface. The poor predictive capacity of model C is not a surprise. The parallel model (model B) seems at first sight to be a reasonable model for the diffusion system, but the experimental data show a very significant deviation from the prediction. The assumption made that no mass transport occurs between the liquid-like and interfacial components must be the reason for the inadequacy of model B. It is suggested that a modified model B (schematically shown in Fig. 10), allowing transport of penetrant molecules across the phase boundary, is physically correct. The interfacial component traps the penetrant molecules and once they reach these domains they spend a significant period of time with few

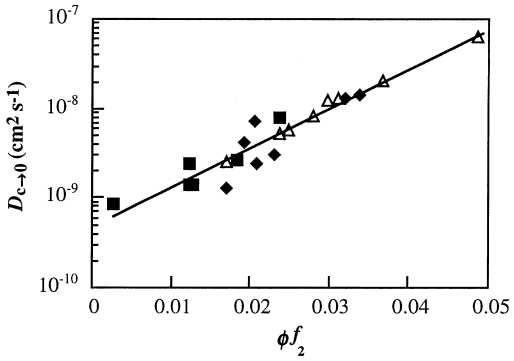

Fig. 13. Zero-concentration diffusivity ($D_{c\to 0}$) as a function of the product of the crystallinity (ϕ; CC + ICC for the heterogeneous poly(ethylene-*co*-octene)s (△) and CC for linear (■) and poly(ethylene-*co*-butene)s (◆)) and the fractional free volume of the penetrable phases (f_2). The data for linear polyethylenes and poly(ethylene-*co*-butene)s are from Hedenqvist et al. [3].

diffusive jumps before entering the mobile liquid-like domains. It does not seem possible at this stage to assess the relative free volume of the interfacial component without molecular dynamics simulation or more coarse-grained simulation techniques (Monte Carlo simulation). However, f_2^{I} must be significantly lower than f_2^{L} (~0.09) because the f_2 values obtained by fitting were near 0.05 (S1) and 0.042 for linear polyethylenes [3]. An interesting possible implication of the modified model B is that larger penetrant molecules would be blocked from entering the interfacial component and hence they would only sense the high free-volume liquid-like component.

4.5. Empirical equation relating diffusivity and mass crystallinity

Data on crystallinity (CC, ICC, IL and L) and zero-concentration diffusivity from the heterogeneous poly(ethylene-*co*-octene)s and earlier data by Hedenqvist et al. [3] on linear polyethylenes and poly(ethylene-*co*-butene)s were combined in all possible ways in order to find a 'universal' relationship for polyethylene. Fig. 13 shows that the zero-concentration diffusivity data could be described by the following expression:

$$D_{\mathrm{Tvo}} = 4.77 \times 10^{-10} \exp(101.47 \phi f_2) \qquad (31)$$

where ϕ is $(1 - w_{\mathrm{CC}})$ for the linear polyethylenes and poly(ethylene-*co*-butene)s and $(1 - w_{\mathrm{CC}} - w_{\mathrm{ICC}})$ for the heterogeneous poly(ethylene-*co*-octene)s. The fitting was very good with a coefficient of correlation $r^2 = 0.988$.

Eq. (31) is a purely empirical equation but its predicative capacity is good. The concentration-dependence of the diffusivity can be introduced according to Eq. (9).

5. Conclusions

The diffusivity data (*n*-hexane in heterogeneous poly(ethylene-*co*-octene)s; hexyl branch contents: 0.8–3.9 mol%) were adequately described by a modified Cohen–Turnbull–Fujita free volume model. The goodness of fit was not critically dependent on the choice of penetrable phases; liquid-like and both interfacial components or liquid-like and IL components. The free volume of the penetrable phases was strongly dependent on their total volume fractions, suggesting the presence of an interfacial penetrable component with low fractional free volume. The dependence of the fractional free volume of the penetrable phases on the phase composition suggests that mass transport takes place from the liquid-like component to the interfacial component, and that the penetrant molecules are trapped at the interfacial sites. The decrease in geometrical impedance factor with increasing crystallinity may be explained by the presence of extraordinarily wide dominant crystal lamellae in the heterogeneous low crystallinity samples. The saturation concentration of *n*-hexane in a wide range of polyethylenes (including both the heterogeneous poly(ethylene-*co*-octene)s and linear polyethylenes and poly(ethylene-*co*-butene)s reported earlier; crystallinity range: 30–94%) showed a complex non-linear dependence on crystallinity that was qualitative in accordance with rubber elasticity theory considering also molecular cilia. Crystal core contents obtained by Raman spectroscopy were lower than the density-based crystallinity, particularly for the samples with the highest degree of branching.

Acknowledgements

This work was sponsored by the Swedish Agency for Research Co-operation with Developing Countries (SAREC) through the joint collaboration of the University of Asmara, Eritrea and the International Science Programs (ISP) of Uppsala University, Sweden.

References

[1] Vieth WR. Diffusion in and trough polymers. Munich: Hanser, 1991.
[2] Hedenqvist M, Gedde UW. Prog Polym Sci 1996;21:299.
[3] Hedenqvist M, Angelstok A, Edsberg L, Larsson PT, Gedde UW. Polymer 1996;37:2887.
[4] Fricke H. Phys Rev 1924;24:575.
[5] Boyd RH. Polym Eng Sci 1979;19:1010.
[6] Michaels AS, Bixler HJ. J Polym Sci 1961;5:413.
[7] Cohen MH, Turnbull D. J Chem Phys 1959;31:1164.
[8] Turnbull D, Cohen MH. J Chem Phys 1970;52:3038.
[9] Fujita H. Fortschr Hochpolym Forsch 1961;3:1.
[10] Kulkarni SS, Stern AS. J Polym Sci, Polym Phys Ed 1983;21:441.
[11] Peterlin A. J Macromol Sci- Phys (B) 1975;28:57.
[12] Fleischer G. Coll Polym Sci 1984;262:919.
[13] Strobl GR, Hagedorn W. J Polym Sci, Polym Phys Ed 1978;16:1181.
[14] Mutter R, Stille W, Strobl GR. J Polym Sci, Polym Phys Ed 1993;31:99.
[15] Mathot VBF, Pijpers MFJ. J Appl Polym Sci 1990;39:979.
[16] Fels M, Huang RYM. J Appl Polym Sci 1979;14:453.
[17] Rogers CE, Stannett V, Szwarc M. J Chem Phys 1959;63:1406.
[18] Bakhouya A, El Brouzi A, Bouzon J, Vergnaud JM. Plast Rubber Compos Process Appl 1993;19:77.

[19] Hedenqvist M, Johnsson G, Tränkner T, Gedde UW. Polym Eng Sci 1996;36:271.
[20] Hedenqvist MS, Gedde UW. Polymer 1999;40:2381.
[21] Hadgett PM, Goldbeck-Wood G, Windle AH. Polymer 2000;41:6151.
[22] Wunderlich B. Macromolecular physics, Crystal structure, morphology, defects, vol. 1. New York: Academic Press, 1973.
[23] Lagarón JM, López-Quintana S, Rodriguez-Cabello JC, Merino JC, Pastor JM. Polymer 2000;41:2999.
[24] Martinez-Salazar, JM, personal communication, 2000.
[25] Vonk CG, Pijpers AP. J Polym Sci, Polym Phys Ed 1985;23:2517.
[26] Kitamaru R, Horii F, Hyon S-H. J Polym Sci, Polym Phys Ed 1977;15:821.
[27] Bergmann K, Nawotki K. Kolloid-Z Z Polym 1967;219:132.
[28] Bergmann K, Nawotki K. Kolloid-Z Z Polym 1972;250:1094.
[29] Bergmann K. Kolloid-Z Z Polym 1973;251:962.
[30] Flory PJ, Rehner J. J Chem Phys 1943;11:521.
[31] Flory PJ. Statistical mechanics of chain molecules. New York: Wiley-Interscience, 1969.
[32] Deblieck RAC, Mathot VBF. J Mater Sci Lett 1988;7:1276.
[33] Williams ML, Landel RF, Ferry JD. J Am Chem Soc 1955;77:3701.
[34] Boyd RH. Macromolecules 1984;17:903.
[35] Olabisi O, Simha R. Macromolecules 1975;8:206.
[36] Stehling FC, Mandelkern L. Macromolecules 1970;3:242.
[37] Crank J. The mathematics of diffusion. 2nd ed. Oxford: Oxford University Press, 1975.